https://doi.org/10.5194/egusphere-2026-4176
Preprint. Discussion started: 20 August 2026

Performance of a 2.05 µm coherent DIAL-Doppler Lidar for CO_2 eddy-covariance turbulent flux measurements

Mathys Thiers[1], Fabien Gibert[2], Julien Lahyani[1], Nicolas Cézard[3]

[1]DOTA, ONERA, Université Paris-Saclay, Palaiseau, 91120, France.
[2]Laboratoire de Météorologie Dynamique (LMD/IPSL), Ecole polytechnique, Institut polytechnique de Paris, Sorbonne Université, Ecole normale supérieure, PSL Research University, CNRS, Ecole 5 des Ponts, Palaiseau, 91120 France
[3]DOTA, ONERA, Université de Toulouse, Toulouse, 3100, France

Correspondence to: Fabien Gibert (gibert@lmd.polytechnique.fr)

Abstract. Understanding the global carbon cycle requires observation of carbon diffusivity within the convective boundary layer (CBL). In particular, observations of the vertical evolution of CO_2 turbulent flux would enable the evaluation of the spatial representativeness of in situ flux measurements and the quantification of entrainment-flux impacts on such measurements. Coherent lidar is a promising technology for this purpose, as it can perform ground-based range-resolved measurements of CO_2 mixing ratio and vertical wind speed along the height of the CBL. Still, achieving a sufficiently low statistical error in the CO_2 mixing ratio measurement is a key challenge in CO_2 turbulent flux measurements. For this purpose, a 2.05 µm coherent differential absorption lidar (CDIAL) has been developed. This lidar features a hybrid fiber/bulk amplification chain that provides 20 kHz high pulse repetition frequency and 1 mJ pulse energy. These characteristics allow for a random error of about 30 ppm in CO_2 mixing ratio measurements and 0.01 m s^{-1} in wind velocity, with a spatiotemporal resolution of 13 s and 115 m, enabling turbulent flux measurements. This paper presents a performance assessment of CO_2 turbulent flux measurements with this CDIAL lidar, under typical meteorological conditions of CO_2 uptake by photosynthesis. A new expression for random error after spatial averaging is introduced, that is verified using Monte Carlo simulations and statistical analysis on experimental measurements. CO_2 fluxes measured by the lidar are discussed with respect to flux measurements made by in situ instruments. The lidar enables flux measurements over the convective boundary layer height (around 1000 m), and achieves a minimum flux detection limit of 11 µmol m^{-2} s^{-1} at a spatiotemporal resolution of 350 m and 4 hours, making it well suited for future geophysical studies of CO_2 turbulent fluxes.

1 Introduction

In the context of global warming, it is essential to accurately monitor the carbon cycle across various spatial and temporal scales to track how ecosystems respond to climate change. Understanding the CO_2 transport processes driven by turbulent fluxes is a key to model the exchanges occurring between the different components of the atmosphere particularly at surface-boundary layer and boundary layer-free troposphere interfaces (Miyazaki et al., 2008).

https://doi.org/10.5194/egusphere-2026-4176
Preprint. Discussion started: 20 August 2026

CO_2 turbulent flux measurements are routinely performed with in situ instruments (sonic anemometers combined with fast-response gas analyzers) using the eddy-covariance method in the FLUXNET network (Delwiche et al., 2024). This technique yields a measurement accuracy of 10 % (Berger et al., 2001); however it suffers from representativeness limitations to small scales (depending on the height of measurement) since in situ ground-based measurements reflect only surface conditions in a small upstream area (the so-called footprint of the flux station). Furthermore, such a network does not provide information on the vertical profile and divergence of fluxes, except occasionally during expensive airborne field campaigns (Hannun et al., 2020).

Lidar measurement techniques have demonstrated the capability to remotely measure turbulent fluxes, with range resolution, throughout the CBL, enabling the investigation of transport processes along the entire CBL. Such lidar-based turbulent flux measurements have been conducted for water vapor fluxes (Sneff et al., 1994; Giez et al., 1999), aerosol fluxes (Engelmann et al., 2007), and sensible and latent heat fluxes (Behrendt et al., 2020). But estimating CO_2 turbulent fluxes from lidar measurements remains challenging due to the requirement on mixing ratio random errors with spatiotemporal resolutions suitable for flux measurements (Gibert et al., 2011). A coherent differential absorption Lidar (CDIAL) lidar operating at a wavelength of 2.05 µm and using elastic backscatter is a promising candidate for achieving sufficiently low random errors in CO_2 mixing ratio measurements to enable turbulent flux estimation. A coherent lidar can perform simultaneous measurements of CO_2 mixing ratio and vertical wind speed, the two physical quantities involved in the eddy-covariance calculation. 2.05 µm CDIAL lidars benefit from strong CO_2 absorption, and from the high backscattered optical signal resulting from high pulse energy achievable with Ho:YLF amplifiers (Lahyani et al., 2024). Still, CDIAL lidars suffer from speckle noise, which limits the signal-to-noise ratio of a single shot to unity. Then, high pulse repetition frequency is therefore required to reduce random error through time-averaging. A first attempt to measure CO_2 turbulent fluxes was conducted by Gibert et al. (2011) using a CDIAL lidar operating at 2.05 µm. The random error in the CO_2 turbulent flux estimate was high (850 % for an average over 6 hour and 1200 m), mainly due to the low pulse repetition frequency (5 Hz) of the lidar. To improve the accuracy of CO_2 mixing ratio measurements, ONERA (Office National d'Étude et de Recherche Aéoronautique) and LMD (Laboratoire de Météorologie Dynamique) have developed together a 2.05 µm CDIAL lidar with high pulse repetition frequency (20 kHz) (Lahyani et al., 2024). The lidar features a hybrid fiber/bulk amplification chain, enabling 1 mJ pulse energy with a duration of 200 ns.

The aim of this paper is to assess the performance of this lidar in measuring CO_2 turbulent fluxes, with a focus on detection limits and measurement biases. Section 2 describes the CDIAL lidar setup and the SIRTA observatory whose data are used to validate our measurements. Section 3 describes the methodology for flux calculations with the CDIAL lidar and the estimation of flux random errors. We derive an expression for the theoretical flux random error after spatial averaging, and we introduce a Monte Carlo-based method to estimate flux random errors. Section 4 reports the experimental performance of the CDIAL lidar for flux measurements. Flux random errors are estimated using two methods: the standard deviation of flux measurements, and the Monte Carlo method introduced in Sect. 3. The latter provides more robust estimates because the standard deviation is calculated from a limited number of measurements. The results obtained with both methods are compared with those

https://doi.org/10.5194/egusphere-2026-4176
Preprint. Discussion started: 20 August 2026

predicted by the analytical expression. A systematic error analysis is also performed. Section 5 discusses the lidar flux measurements with respect to in situ measurements and geophysical conditions.

2 Instruments

2.1 DIAL Doppler lidar at 2.05 µm

The 2.05 µm CDIAL used for vertical wind speed and CO_2 mixing ratio measurements is presented in Fig. 1. The laser source of the lidar is described in Lahyani et al. (2024). It features a Master Oscillator Power Amplifier (MOPA) architecture composed of four single-pass fibered amplifiers – one continuous-wave amplifier and three pulsed amplifiers – based on thulium doped fiber, and one single-pass bulk amplifier using a Ho:YLF crystal. This amplification chain is seeded by two external-cavity diode lasers (ECDLs) which emit continuous signals at the wavelengths λ_{ON} and λ_{OFF} used for DIAL measurements. The wavelengths λ_{ON} and λ_{OFF} are respectively positioned on and outside the R30 CO_2 absorption line. A portion of the signal at λ_{ON} is tapped and directed to a wavemeter in order to continuously monitor λ_{ON}. An optical switch sequentially directs the two seed lasers into the amplification chain. An acousto-optic modulator shapes the continuous signal from seed lasers into 200 ns pulses. The MOPA architecture provides flexibility in adjusting the pulse repetition frequency without altering pulse duration, making it well suited to operate at 20 kHz with the desired 200 ns pulse duration. The pulse energy at the output of the lidar is 1 mJ. The lidar uses a monostatic telescope with a beam expander whose aperture diameter is 76 mm. The backscattered signal is directed toward the detection chain using a circulator composed of a dielectric polarization beam splitter and a quarter-wave plate. The backscattered signal is mixed with a local oscillator – tapped after the continuous-wave amplification – using a 95/5 fiber coupler.

Table 1 : Technical specifications of the CDIAL lidar.

Transmitter		**Receiver**	
Pulse Energy	1 mJ	Lens Aperture	76 mm
Pulse duration	200 ns	Local oscillator Power	0.7 mW
Beam quality factor (M^2)	1.2	Detector Sensitivity Noise Equivalent Power	InGaAs PIN photodiode 1.2 $A.W^{-1}$ 8 $pW.Hz^{-1/2}$
Wavelengths	λ_{ON} 2050.96 nm λ_{OFF} 2051.25 nm		
Pulse Repetition Frequency Wavelengths switch frequency	20 kHz 0.6 kHz	Signal Processing	Real time 256-ns time gate (38.4-m range gate). Discrete Fourier Transform accumulation over 0.1 s (1000 pair shot). Spectral estimator.

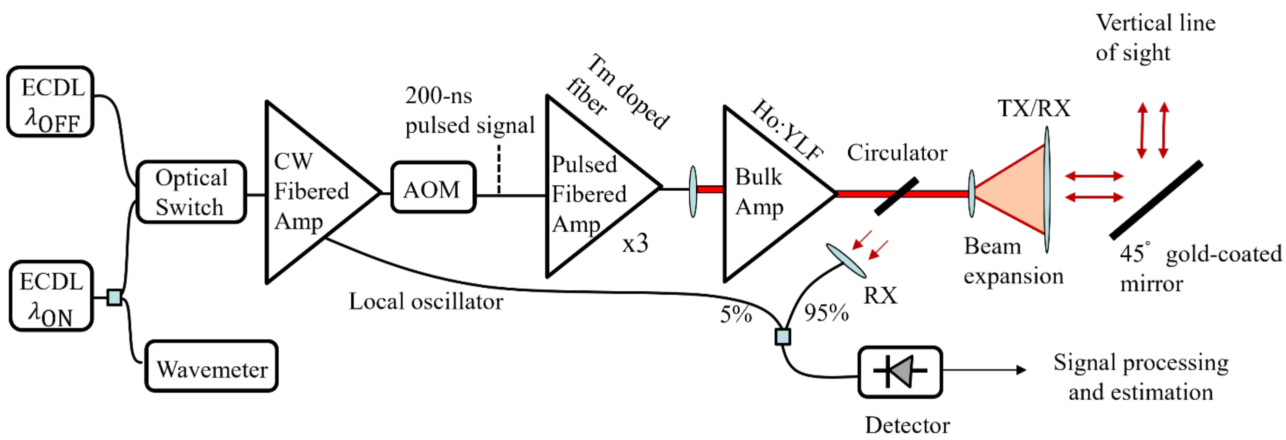

Figure 1 : Optical Setup of the 2.05 µm CDIAL lidar. Abbreviations: External Cavity Diode Laser ECDL (ECDL), continuous (CW), amplifier (Amp), acousto-optic modulator (AOM), Thallium (Tm), transmitter (TX), receiver (RX).

The resulting heterodyne signal is then detected using an InGaAs photodiode. Table 1 summarizes the technical specifications. The signal processing procedure used to retrieve the CO_2 mixing ratio is described in Gibert et al. (2006). The backscattered signal is accumulated over range gates of $\Delta R = 38$ m along the line of sight. For each range gate, the power of the heterodyne current at both wavelengths, P_{OFF} and P_{ON} , is calculated using a power estimator. The power estimator consists of computing the power spectral density (PSD) of the heterodyne signal, removing the noise by subtracting the PSD of a far range gate, and integrating the PSD around the signal peak. We use an integration bandwidth of 24 MHz.

The absorption cross-sections at the two wavelengths $\tilde{\sigma}_{\mathrm{ON}}$ and $\tilde{\sigma}_{\mathrm{OFF}}$ are calculated using spectroscopic data from the HITRAN database with an algorithm that computes the Voigt-Van-Vleck-Huber profile of the CO_2 absorption line. These calculations use the real-time value of λ_{ON} provided by the wavemeter, as well as the temperature and pressure measurements from the 50 m meteorological mast at the SIRTA observatory.

2.2 In situ data at SIRTA observatory

At SIRTA Observatory, an in situ eddy-covariance station was used to support the CO_2 turbulent flux measurements obtained with the lidar. The station operates at a height of 50 m and is located approximately 2 km away from the lidar site. It provides measurements of vertical wind speed, CO_2 mixing ratio, temperature, pressure and humidity at a time resolution of 0.1 s, using a LICOR LI-7200 gas analyser and a METEK uSonic-3 sonic anemometer (Haeffelin et al., 2005). The station also delivers temperature and humidity profiles throughout the height of the CBL using a microwave radiometer (HATPRO-G2) and a 3D wind profile spanning the CBL using a UHF radar. This station provides four types of information relevant to our analysis: the atmospheric parameters (pressure, temperature, and humidity) that are required for computing the CO_2 mixing ratio, a reference

https://doi.org/10.5194/egusphere-2026-4176
Preprint. Discussion started: 20 August 2026

of CO_2 turbulent flux measurement, some quantities (CO_2 atmospheric fluctuations and integral scales) that are required to determine the sampling error of the flux but cannot be measured by lidar, and the temperature and humidity turbulent fluxes, which constitute sources of bias in the lidar-derived CO_2 flux estimates.

3 Methodology

3.1 CO_2 mixing ratio and vertical wind retrieval with the CDIAL lidar

After the range-resolved measurement of the backscattered powers P_{OFF} and P_{ON} (A^2), the differential absorption optical depth $\tau(z_i)$ is estimated at a range z_i with:

$$\tau(z_i) = \frac{1}{2}\ln\left(\frac{P_{\mathrm{OFF}}(z_i)}{P_{\mathrm{ON}}(z_i)}\right) \quad (1)$$

The differential absorption α (m^{-1}) is estimated over a 115-m range gate using a linear regression applied to three consecutive measurements of τ. The CO_2 mixing ratio $x_{\mathrm{CO_2}}$ (ppm) is then derived using the following expression:

$$x_{\mathrm{CO_2}}(z_i) = \frac{1}{\rho_{\mathrm{d}}(z_i)(\tilde{\sigma}_{\mathrm{ON}}(z_i) - \tilde{\sigma}_{\mathrm{OFF}}(z_i))}\alpha(z_i) \quad (2)$$

where ρ_{d} ($\mathrm{mol\ m^{-3}}$) is the dry air density, $\tilde{\sigma}_{\mathrm{ON}}$ and $\tilde{\sigma}_{\mathrm{OFF}}$ ($\mathrm{m^2}$) are the absorption cross-sections at the respective wavelengths. The dry air density is given by:

$$\rho_{\mathrm{d}}(z_i) = \frac{p(z_i)}{N_{\mathrm{A}} k_{\mathrm{b}} T(z_i)} \frac{1}{1 + q(z_i)\frac{M_{\mathrm{d}}}{M_{\mathrm{H_2O}}}} \quad (3)$$

where p (Pa) is the pressure, N_{A} ($\mathrm{mol^{-1}}$) is the Avogadro's Number, T (K) the temperature, k_{b} ($\mathrm{J\ K^{-1}}$) the Boltzmann constant, q ($\mathrm{g\ kg^{-1}}$) the specific humidity, M_{d} ($\mathrm{mol^{-1}}$) the molar mass of dry air and $M_{\mathrm{H_2O}}$ ($\mathrm{mol^{-1}}$) the molar mass of water. The variables p, T and q are obtained from SIRTA observatory measurements throughout the height of the CBL. Assuming a linear variation of temperature with altitude, following the profile described in Di Girolamo et al. (2004), we apply a linear regression to the temperature data over the CBL height. Specific humidity is assumed to be vertically uniform, consistent with a well-mixed CBL (Gibert et al., 2026), using the averaged value over the CBL. Pressure is derived from the hydrostatic equilibrium equation, using the pressure measured at 50 m as the lower-boundary condition.

The vertical wind speed is measured by the CDIAL lidar, using classical coherent Doppler anemometry. For a vertical line of sight, the expression of the vertical wind velocity w ($\mathrm{m\ s^{-1}}$) is:

$$w(z_i) = -\frac{\lambda}{2}\Delta f(z_i) \quad (4)$$

where Δf (Hz) is the Doppler frequency shift induced by aerosol motion in the backscattered signal. More precisely, $\Delta f(z_i)$ is an average of the frequency shift that occurs on the three range gates of 38 m used to compute $x_{\mathrm{CO_2}}$ at the elevation z_i.

https://doi.org/10.5194/egusphere-2026-4176
Preprint. Discussion started: 20 August 2026

3.2 Flux calculation

The CO_2 turbulent flux is calculated using the eddy-covariance method, following the formalism described in Behrendt et al. (2020). First, CO_2 mixing ratio and vertical wind speed data measured by the CDIAL lidar are cleaned of outliers. It means that for each height and period measurement, the data outside of 3 standard deviations from the mean are removed. Then, CO_2 mixing ratio fluctuations $x'_{\mathrm{CO_2}}$ and vertical wind speed fluctuations w' are estimated using a detrending procedure applied to the lidar measurements. Detrending is performed by removing a linear trend computed over the flux measurement period from the measurement time series. The procedure aims to remove synoptic scale contributions so that only turbulent fluctuations remain. The flux at height z_i is computed using:

$$F_{\mathrm{CO_2}}(z_i) = \rho_{\mathrm{d}} \frac{1}{N(z_i)} \sum_{i=1}^{N(z)} w'(z_i) x'_{\mathrm{CO_2}}(z_i) \quad (5)$$

where, $F_{\mathrm{CO_2}}$ (mol m^{-2} s^{-1}) is the flux, and $N(z_i)$ is the number of temporal measurements used at height z_i, which varies due to outlier elimination.

3.3 Flux random error prediction

Achieving a sufficiently low level of random error is the main challenge in measuring CO_2 turbulent fluxes using lidar. In this subsection, we present the methods used to predict this random error. An important step in reducing the random error is the vertical averaging of flux measurement. We introduce an expression for the random error after vertical averaging based on the spatial correlation between flux measurements. In addition, we estimate flux random errors using Monte Carlo simulations based on the lidar data. This approach allows us to validate the expression of the random error after vertical averaging introduced here.

3.3.1 Random error estimate of a single eddy flux calculation

The random error of a turbulent flux measurement by eddy-covariance has two components, the instrumental error and the sampling error, such as (Giez et al., 1999):

$$\sigma_{\mathrm{tot},F} = \sqrt{\sigma_{\mathrm{n},F}^2 + \sigma_{\mathrm{s},F}^2} \quad (6)$$

where $\sigma_{\mathrm{n},F}$ and $\sigma_{\mathrm{s},F}$ (mol m^{-2} s^{-1}) are the standard deviations of the instrumental and sampling errors respectively, and $\sigma_{\mathrm{tot},F}$ (mol m^{-2} s^{-1}). the standard deviation of the total random error.

The sampling error quantifies the lack of temporal representativeness in the flux measurement due to the finite measurement duration T (s). Its expression is given by (Lenschow et al., 1994):

$$\sigma_{\mathrm{s},F} = \frac{2\min(l_w^{\mathrm{t}}, l_{x_{CO_2}}^{\mathrm{t}})}{T} \sqrt{F_{\mathrm{CO_2}}^2 + \rho_{\mathrm{d}}^2 \sigma_{\mathrm{a},x_{\mathrm{CO_2}}}^2 . \sigma_{\mathrm{a},w}^2} \quad (7)$$

where $\sigma_{\mathrm{a},x_{\mathrm{CO_2}}}$ (ppm) is the standard deviation of the atmospheric fluctuation of $x_{\mathrm{CO_2}}$, $l_{x_{\mathrm{CO_2}}}^{\mathrm{t}}$ (s) and l_w^{t} (s) are the integral time scales for $x_{\mathrm{CO_2}}$ and w turbulent fluctuations, respectively.

https://doi.org/10.5194/egusphere-2026-4176
Preprint. Discussion started: 20 August 2026

The second flux error component is the instrumental error, which results from the instrumental error on x_{CO_2} and w measurements. As described in Appendix A, we can simplify the expression by noting that the noise on x_{CO_2} is much larger than the atmospheric fluctuations of x_{CO_2}, while the noise on w is much smaller than its atmospheric fluctuations. The simplified expression is (Giez et al., 1999):

$$\sigma_{\mathrm{n},F}(z_i) = \rho_{\mathrm{d}}\sqrt{\frac{\Delta t}{T}}\,.\,\sigma_{\mathrm{n},x_{CO_2}}(z_i)\,.\,\sigma_{\mathrm{a},w}(z_i) \quad (8)$$

where Δt (s) is the temporal resolution of lidar measurements (13 s), T (s) is the time resolution of eddy covariance flux measurement, $\sigma_{\mathrm{n},x_{CO_2}}$ (ppm) is the instrumental noise standard deviation of x_{CO_2} and $\sigma_{\mathrm{a},w}$ (m s^{-1}) is the atmospheric turbulence standard deviation of w.

The natural and instrumental variance and the integral scale of vertical wind speed can be estimated accurately using lidar measurements. We compute these parameters using the methods described in Wulfmeyer et al. (2016). First, the autocovariance function of wind speed data is computed, as a function of lag time τ. Then, the autocovariance function is fitted with a $-\tau^{2/3}$ dependency model (Kolmogorov turbulence inertial range) with lag time. The origin of the fitted function is the atmospheric wind variance with no more contribution of instrumental noise. We use the integral up to first zero crossing of the fitted autocovariance function to calculate the time integral scale of wind speed. In addition to flux random error prediction, computing integral scale allows to know the largest time for which lidar data can be averaged. Unfortunately, we cannot use the same formalism to estimate natural variance and integral scale of CO_2 turbulent fluctuations in Eq. (7), as x_{CO_2} data are usually too noisy with respect to natural atmospheric fluctuations. In this study we assume that $l_w^{\mathrm{t}} = \min(l_w^{\mathrm{t}}, l_{x_{CO_2}}^{\mathrm{t}})$ as it is generally observed (Gibert et al., 2011) and use lidar measurements of l_w^{t} for error computation. We also use the value of F_{CO_2} and $\sigma_{\mathrm{a},x_{CO_2}}$, provided by in situ measurements performed at 50 m height on the day of the case study (15 May 2025).

3.3.2 Random error expression for a vertically averaged flux

The random error can be reduced by spatially averaging turbulent flux measurements:

$$\langle F_{CO_2}\rangle_{z_{\min}}^{z_{\max}} = \frac{1}{k}\sum_{z_i=z_{\min}}^{z_{\max}} F_{CO_2}(z_i) \quad (9)$$

where $\langle F_{CO_2}\rangle_{z_{\min}}^{z_{\max}}$ (mol m^2 s^{-1}) is the turbulent flux averaged between the height $z_{\min}$ and $z_{\max}$, and k is the number of averaged flux. The spatial correlation of the flux random error must be known to derive the expression of the random error after spatial averaging. We note that the instrumental noise in x_{CO_2} exhibits a particular spatial correlation structure due to the derivative estimator applied to the optical depth (3 points in our case). It appears that the noise of x_{CO_2} is spatially uncorrelated except for the second nearest neighbour of a given measurement for which there is an anti-correlation. The derivation of the spatial correlation of the x_{CO_2} noise is presented in Appendix B. We assume that the spatial correlation of the flux random error is fully determined by the spatial correlation of the random error of x_{CO_2}. In Appendix A, we demonstrate that this assumption holds if the vertical variability of wind speed can be neglected. This assumption thus implies a strong vertical correlation of

https://doi.org/10.5194/egusphere-2026-4176
Preprint. Discussion started: 20 August 2026

wind speed, which is supported by the vertically coherent structure of thermal updrafts and downdrafts (see Sect. 4.1, Fig. 2b). Knowing the spatial correlation of flux measurements, we can deduce the random error after spatial averaging $\langle\sigma_{\mathrm{n},F}\rangle_{z_{\min}}^{z_{\max}}$ (mol m^2 s^{-1}), which is given by (see Appendix A):

$$\langle\sigma_{\mathrm{n},F}\rangle_{z_{\min}}^{z_{\max}} = \frac{1}{k}\sqrt{\sigma_{\mathrm{n},F}^2(z_{\min}) + \sigma_{\mathrm{n},F}^2(z_{\max})} \qquad (10)$$

In this study, we apply this simplified model, in which the vertical variability of vertical wind speed is neglected, and compare the results with flux error estimates derived from Monte Carlo simulations.

Contrary to the instrumental error, vertical averaging may not lead to a reduction in sampling error. Indeed, the largest eddy scales affect all flux measurements along the line of sight in a similar way, resulting in the same lack of representativeness across the measurements. Therefore, a conservative approach is to consider that the standard deviation of the sampling error after vertical averaging $\langle\sigma_{\mathrm{s},F}\rangle_{z_{\min}}^{z_{\max}}$ is the maximum of the sampling error of flux measurements in the averaging area.

$$\langle\sigma_{\mathrm{s},F}\rangle_{z_{\min}}^{z_{\max}} = \max_{z_{\min}\le z_i\le z_{\max}} \sigma_{\mathrm{s},F}(z_i) \qquad (11)$$

3.3.3 Determination of instrumental random error on flux with Monte Carlo simulations

The second approach for determining the random error is a Monte Carlo simulation based on the random shuffle method (denoted as RS method). This method allows for a determination of the instrumental error directly from the lidar data. It also enables an assessment of data quality by verifying that the instrumental error obtained with the Monte Carlo simulations agrees with that predicted by the analytical expressions. In addition, the Monte Carlo simulations allow us to validate the expression of the random error after spatial averaging introduced in the previous subsection. The RS method was introduced by Billesbach et al. (2011). It consists in computing the covariance between $x'_{\mathrm{CO_2}}$ and w' after randomly shuffling one of the two time series. This process is repeated for a large number of shuffles, allowing a Monte Carlo estimation of the standard deviation of the flux. It has been objected that this method can overestimate the instrumental error because atmospheric fluctuation of $x_{\mathrm{CO_2}}$ is considered as a part of the error due to instrumental noise (Rannik et al., 2016). Nevertheless, this overestimation should not be significant in our case because instrumental noise is the dominant contribution to $x_{\mathrm{CO_2}}$ fluctuations. In this study, we shuffle the $x_{\mathrm{CO_2}}$ measurements and compute their covariance with unshuffled wind data. We apply the same shuffling at all measurement elevations in order to not alter the spatial correlation of instrumental noise. It allows us to evaluate the standard deviation after spatial averaging using RS method and to compare the result with the analytical expression presented in Sect. 3.3.2.

https://doi.org/10.5194/egusphere-2026-4176
Preprint. Discussion started: 20 August 2026

4 Results of performance of CO_2 turbulent flux measurement with the DIAL-Doppler lidar

4.1 Meteorological and turbulent conditions: integral scales and lidar resolution justification

The measurements used for our investigation were conducted on 15 May 2025, between 12:00 and 16:00 local time at ONERA in Palaiseau, France. Figure 2a shows the Carrier to Noise Ratio (CNR) profiles obtained during the measurement period, with the CBL height indicated by the black dotted line. The CBL height is identified by the intense peak in CNR followed by a sharp decrease; we use the first maximum of the CNR derivative to determine the height, which corresponds to the bottom of the CBL. The CBL height remains close to 850 m with a slight rise during the measurement period. Figure 2b shows the evolution of wind speed during the measurement. Figures 2c and 2d display the vertical profiles of wind speed variance and temporal integral scale averaged over the 4-hour measurement period.

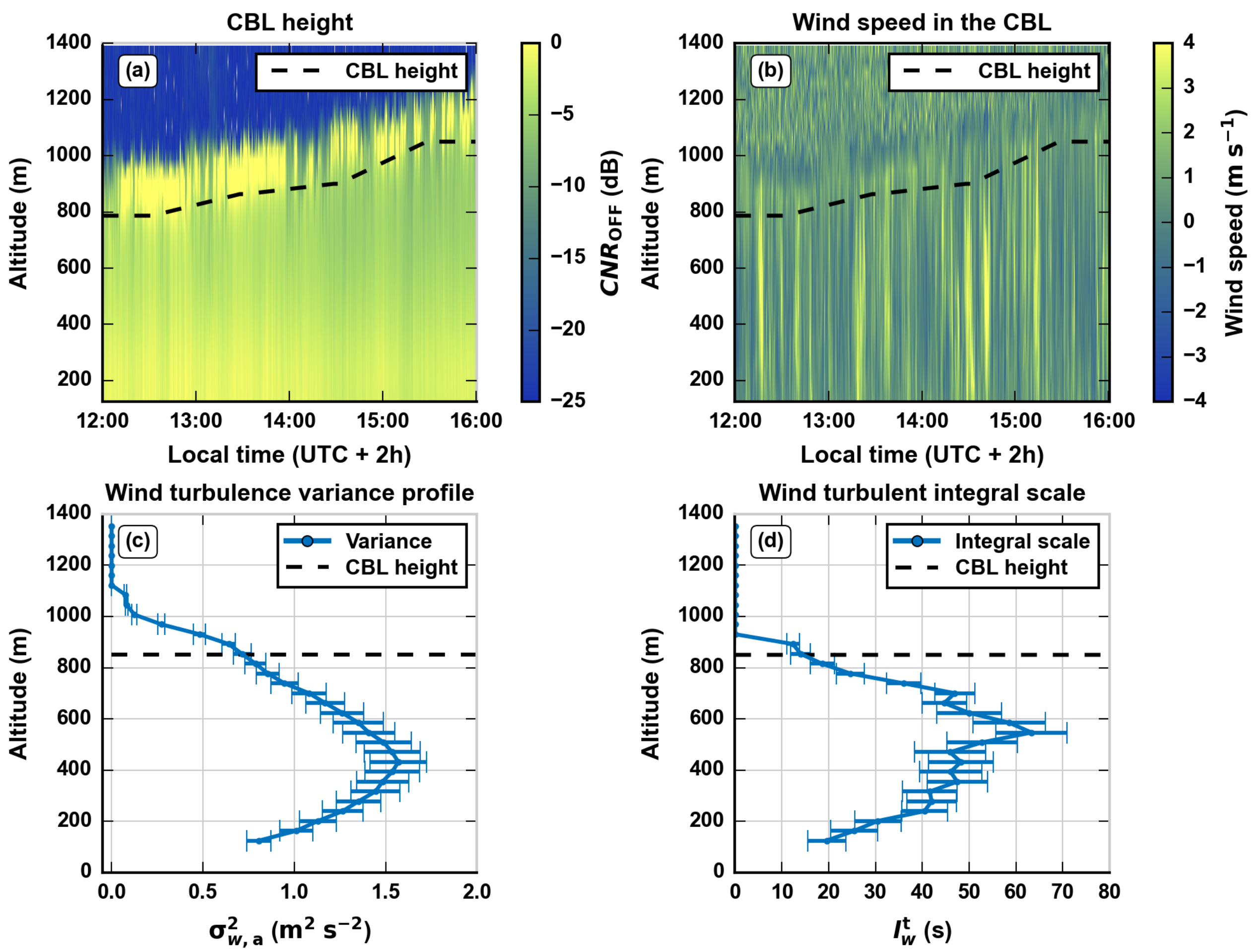

Figure 2 : a) Backscattered signal at the wavelength λ_{OFF}. The CBL height is indicated in black dotted line. b) Wind speed measurements, a positive velocity denotes an upward wind c) Wind turbulence variance profile. d) Wind turbulent integral scale profile. The variance and turbulent scale profiles are computed using a 30-min time window and averaged over the 4-hour measurement period. CBL : convective boundary layer.

https://doi.org/10.5194/egusphere-2026-4176
Preprint. Discussion started: 20 August 2026

These profiles exhibit a maximum around the mid-height of CBL which is consistent with the similarity theory (Stull, 1988). The temporal and spatial integral scale profiles provide the characteristic time and space scales of atmospheric turbulences, thereby guiding the appropriate selection of lidar spatiotemporal resolution. The spatiotemporal resolution must be smaller than the temporal and spatial integral scales of the flux in order to keep a bias under 10 % (Gibert et al., 2011) on flux measurements. The integral scales of the flux is assumed to be equal to the wind speed integral scale as it is considered smaller than $x_{\mathrm{CO_2}}$ integral scale (see Sect. 2.3.1). According to Fig. 2d, the limiting value is the one measured at the lowest elevation: $l_w^{\mathrm{t}} = 20$ s. The estimation of the spatial integral scale l_w^{z} is difficult because the CBL height restricts the available measurement window over which a spatial autocovariance function can be computed. The problem becomes more pronounced near the boundaries of the measurement domain. We can estimate it with Taylor's hypothesis, $l_w^{\mathrm{z}} = U l_w^{\mathrm{t}}$ (Lenschow et al., 2000), where U (m s^{-1}) is the horizontal wind speed. We adopt the value of $U = 7.75$ m s^{-1} measured by the SIRTA observatory at a height of 200 m, which yields $l_w^{\mathrm{z}} = 155$ m. Consequently the spatiotemporal resolution of 115 m and 13 s employed in this paper meets the requirements imposed by the integral scales.

4.2 Lidar CO_2 and wind measurement performances

CO_2 mixing ratio and vertical wind speed measurements are affected by instrumental errors, mainly due to the shot noise and the relative intensity noise of the local oscillator, and to the detector noise. These instrumental errors contribute to the statistical uncertainty of the turbulent flux measurements. We estimate the instrumental errors by computing the power spectral density of the measurement series and isolating the high frequency noise floor. We compare these instrumental error estimates with the Cramér-Rao bound (CRB) whose expression is given by Rye et al. (2000). The CRB is computed from the experimental values of CNR. The results of instrumental errors are presented Fig. 3a and Fig. 3b.

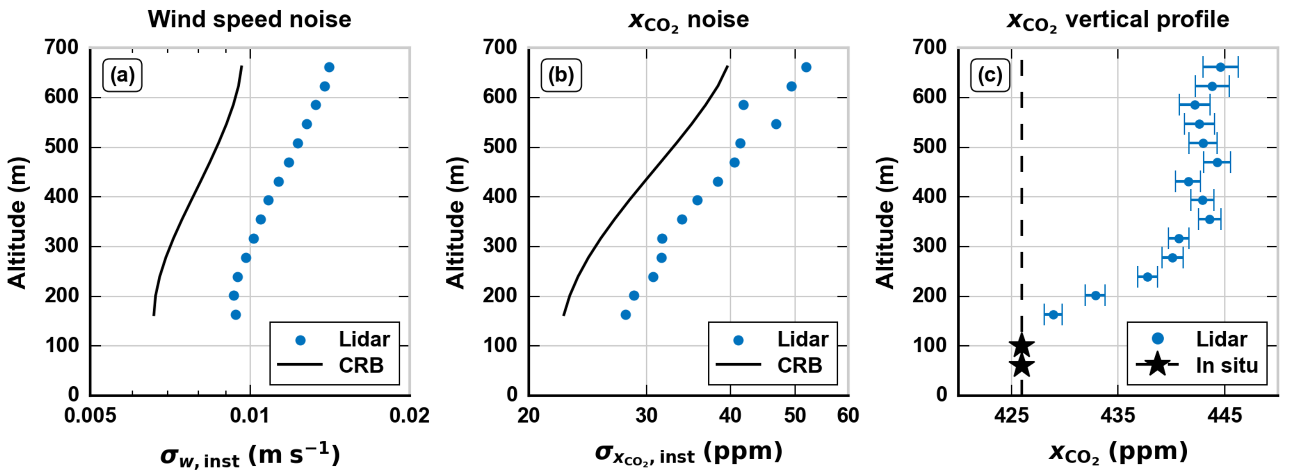

Figure 3 : Performances of lidar measurements a) vertical wind speed noise at spatiotemporal resolution of flux measurement (Δt = 13 s and Δz = 115 m). b) $x_{\mathrm{CO_2}}$ noise at spatiotemporal resolution of flux measurement (Δt = 13 s and Δz = 115 m). c) 4-hour $x_{\mathrm{CO_2}}$ average. CRB : Cramér-Rao Bound.

https://doi.org/10.5194/egusphere-2026-4176
Preprint. Discussion started: 20 August 2026

The experimental results are close to the CRB – within 25 % and 40 % for x_{CO_2} and w respectively – and follow the predicted trend. We note that the statistical error of wind speed measurements is much smaller than the amplitude of atmospheric turbulence (Fig. 3a) and therefore contributes negligibly to the overall random error of the flux estimates. We determine the systematic errors affecting x_{CO_2} measurements by averaging the measurements over a period of 4 hours. Figure 3c shows that the temporal average of CO_2 mixing ratio increases with altitude, reaching a deviation of 5 % compared to the reference in-situ measurements. These in situ measurements are performed by the ICOS station of Saclay, located 7 kilometers away from the lidar site (Ramonet et al., 2026), and do not exhibit any increase between the two measurement levels (60 m and 100 m). Assuming a well-mixed CBL, the increase described by lidar-derived measurements must therefore be attributed to an instrumental bias. The potential sources of systematic errors in the CO_2 mixing ratio measurement are presented in Table 2. These include bias in the positioning of λ_{ON}, overlap of the R30 absorption line with an absorption line of H_2O, and deviations of atmospheric parameters from the assumed profile (see Sect. 3.1). We consider a deviation of 1 K (10 % of the vertical evolution within the CBL) and a deviation of 0.6 g kg^{-1} (10 % of the humidity in the CBL). Pressure is a negligible source of bias when λ_{ON} is positioned at the top of the absorption line (Gibert et al., 2008), and is therefore not considered. These sources of bias appear insufficient to explain the observed 18 ppm deviation between the lidar and the instrument, which suggests that an instrumental bias source remains to be identified in future works. Nevertheless, the bias remains under 5 % of the mean mixing ratio. Consequently, if this bias also applies to x'_{CO_2} fluctuations, then it would induce a bias of less than 5 % in the turbulent flux, which is an acceptable performance for this first measurement. If it applies only on x_{CO_2} values as a fixed term (constant bias), then it is suppressed during the detrending operation presented in Sect. 3.2, and it does not induce any bias on flux measurements.

Table 2 : Assessment of potential systematic errors on the CO_2 mixing ratio measurement

Parameters	Bias	Reference and comments
λ_{ON} positioning	< ± 3 ppm	Considering the 40-MHz precision of the wavemeter
H_2O absorption line overlap	< + 0.2 ppm	From Gibert et al. (2006). Considering a differential absorption cross-section of water of 1.2 10^{-30} m^2 and a specific humidity of 6 g kg^{-1}.
Bias on atmospheric parameters: Humidity Temperature	 < ± 0.7 ppm < ± 0.5 ppm	The sensitivities of the CO_2 measurements to temperature and humidity are reported in Appendix C. We consider a bias in the atmospheric parameters of $T' = 1$ K, and $q' = 1$ g kg^{-1}.

4.3 Random error of CO_2 turbulent flux

Random error is the critical aspect in the measurement of CO_2 turbulent flux with a CDIAL lidar. In this subsection, we apply the methodology presented in Sect. 3.3 to our experimental dataset, in order to assess the flux detectability of the lidar.

https://doi.org/10.5194/egusphere-2026-4176
Preprint. Discussion started: 20 August 2026

We first compute the theoretical sampling error using Eq. (7). However, the parameters $\sigma^2_{\mathrm{a},x_{\mathrm{CO_2}}}$ and $l^{\mathrm{t}}_{x_{\mathrm{CO_2}}}$ cannot be estimated with the lidar because the random error is too large. We therefore use the sampling error obtained at 50-m height with the data of the SIRTA observatory, at the elevations of lidar measurements. We consider that the minimum between the integral scales is l^{t}_{w} as it is the general case (Gibert et al., 2011; Giez et al., 1999). So, we compute the sampling error at each measurement altitude using the measurement of $\sigma_{\mathrm{a},w}(z_i)$ and $l^{\mathrm{t}}_{w}(z_i)$ provided by the lidar, but using the value of $F_{\mathrm{CO_2}} = 25$ µmol m^{-2} s^{-1} and $\sigma_{\mathrm{a},x_{\mathrm{CO_2}}} = 1.5$ ppm measured by the SIRTA at 50 m.

The theoretical instrumental error is computed using Eq. (8), using the measurement of $\sigma_{\mathrm{n},x_{\mathrm{CO_2}}}$ and $\sigma_{\mathrm{a},w}$ provided by the lidar. We also obtain an estimate of the instrumental error using the RS method (see Sect. 3.4.3).

Then, we compute the total random error by combining the two components at each altitude (Eq. (6)). Therefore, there is a single procedure to estimate the sampling error, whereas the instrumental error can be derived from either the analytical expression or the RS method.

We compare these predicted random errors to experimental results. During the measurement period – an interval of 4 hour from 12:00 to 16:00 local time – we performed eight eddy-covariance calculations using 30-minute time windows at each measurement altitude. We evaluate the standard deviation $\sigma_{F_{\mathrm{CO_2}},30\mathrm{min}}$ of this series of eight measurements, and we extrapolate this standard deviation to a 4-hour period with:

$$\sigma_{F_{\mathrm{CO_2},4\mathrm{h}}} = \frac{\sigma_{F_{\mathrm{CO_2},30\mathrm{min}}}}{\sqrt{M}} \quad (12)$$

where $\sigma_{F_{\mathrm{CO_2},4\mathrm{h}}}$ is the standard deviation extrapolated and M is the number of 30-minute flux measurements (equals 8 in this study).

The total random errors are reported Fig. 4a. In this figure, "MCS" denotes the Monte Carlo simulation results, while "theory" refers to the results derived from analytical expressions. We indicatively displayed the contribution of the sampling error with the orange dotted line, and we see that it represents a negligible contribution to the total random error.

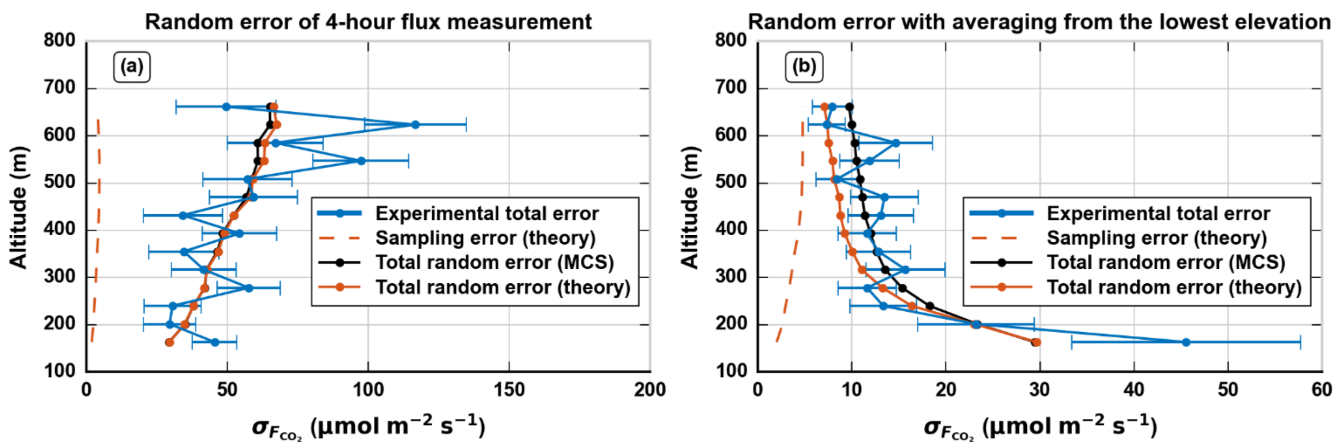

Figure 4 : Flux random error determination a) per altitude at 115-m spatial resolution b) with vertical averaging between the lowest elevation and the elevation at the y-axis reference point. MCS : Monte-Carlo simulations.

https://doi.org/10.5194/egusphere-2026-4176
Preprint. Discussion started: 20 August 2026

We find that the random errors predicted by the analytical expression and by the RS method both agree with the experimental estimates. This supports the validity of these three approaches for investigating the random error in turbulent fluxes. To investigate the effect of vertical averaging on the reduction of random error, we compute the random error of the 4-hour flux measurements as fluxes are progressively averaged vertically starting from the lowest elevation. The results are shown in Fig. 4b. The sampling error is taken as the maximum sampling error value included within the considered altitude range. The theoretical instrumental error is computed from the analytical expression presented Eq. (10). The instrumental error is also estimated using the RS method by averaging the flux computed from shuffled data at the different measurement altitudes. Data are shuffled identically at each altitude to preserve the vertical correlation. The instrumental and sampling errors are then combined to obtain the total random error. In addition, the experimental total random error is derived from the standard deviation of eight 30-min flux estimates spatially averaged over the considered altitudes. We find that the random errors predicted by the analytical expression and by the RS method both agree with the experimental estimates. This supports the correlation-based approach used to derive the expression for the random error after vertical averaging. The random error provided by the RS method is about 20 % higher than that provided by the analytical expression, and shows better agreement with the experimental results. The RS method, based on lidar data, may account for some aspects neglected in the analytical expression, such as the vertical evolution of wind turbulences. We use the results of this method in this paper to estimate the flux random errors. We see that after vertical averaging over the lower half of the CBL, at a height of 450 m, the random error is 11 µmol m^{-2} s^{-1}, meaning that the lidar can detect fluxes above this value with spatiotemporal resolutions of 350 m and 4 hours. This detectability enables the lidar to measure fluxes driven by photosynthesis.

4.4 Biases on CO_2 turbulent flux measurements

A first source of bias on turbulent flux measurement arises from the limited spatiotemporal resolution of the lidar which acts as a low-pass filter on the atmospheric turbulence spectrum. As the temporal resolution of lidar measurements is lower than the temporal integral scale of vertical wind speed (see Sect. 4.1) by a factor between 2 (for $z < 200$ m and $z > 750$ m) and 5 (for 300 m $< z <$ 700 m), the resulting bias is likely to be limited to a few percent of the total flux (Gibert et al., 2011). To estimate this bias, we used the in situ flux station data at 50-m height and performed temporal averaging to degrade the time resolution to the integral scale divided by 2 and 5. For an integral scale of 4 s at 50 m this corresponds to temporal resolutions of 2 s and 0.8 s. The bias on eddy-covariance flux was respectively 8 %, (i.e. 1.8 µmol m^{-2} s^{-1}) and 2 % (i.e. 0.5 µmol m^{-2} s^{-1}). Thus, 8 % is expected to be an upper bound for the bias induced by the low resolution of lidar data.

In addition, temperature and humidity turbulent fluxes introduce biases in turbulent CO_2 flux estimates. Fluctuations in temperature and humidity induce fluctuations in dry air density and modify the CO_2 absorption through changes in the absorption cross-section (Webb et al., 1980). Let X denote either the specific humidity q (g kg^{-1}) or the temperature T (K). The turbulent flux associated to X, F_X, is defined as:

$$F_X = \frac{1}{N}\sum_{i=1}^{N} w'(i)X'(i) \tag{13}$$

https://doi.org/10.5194/egusphere-2026-4176
Preprint. Discussion started: 20 August 2026

It can be shown that the fluxes of these quantities introduce a bias $F_{\mathrm{b},X}$ (mol m^{-2} s^{-1}) on the CO_2 turbulent flux measurement given by (see Appendix C):

$$F_{\mathrm{b},X} = \rho_{\mathrm{d}} S_X F_X \tag{14}$$

where S_X is the sensitivity of $x_{\mathrm{CO_2}}$ measurement to the parameter X. S_X quantifies the bias introduced in $x_{\mathrm{CO_2}}$ per unit change of X.

To estimate these biases, profiles of sensible and latent heat flux are ideally required, but were not available for this study. Therefore, we estimated these fluxes using the 50-m height measurements from the SIRTA observatory, temporally averaged over the lidar measurement period. The results are provided in Table 3.

Table 3 : Bias on CO_2 turbulent flux at low altitude. Biases are estimated using in situ data at 50-m height and are to be compared to the averaged CO_2 flux over the lidar measurement period, i.e. -25 µmol m^{-2} s^{-1}.

Parameter	Bias	Comments
Lidar low pass filtering in turbulence spectrum	$F_{\mathrm{b}} \sim +1.8$ µmol m^{-2} s^{-1} at $z = 100$ m $F_{\mathrm{b}} \sim +0.5$ µmol m^{-2} s^{-1} at $z = 400$ m	using Fig. 2d and inferred from in situ data at $z = 50$ m.
Bias on $x_{\mathrm{CO_2}}$ measurement determined in Sect. 4.2	$F_b < -1.25$ µmol m^{-2} s^{-1}	< 5 % of the value at 50 m height.
Biases from humidity and temperature fluctuations		
Humidity: Sensitivity of x_{CO_2} measurement: 50-m height turbulent flux Resulting bias	 $S_q = -0.66$ ppm g^{-1} kg $F_q = +0.04$ g kg^{-1} m s^{-1} $F_{\mathrm{b},q} = -1.1$ µmol m^{-2} s^{-1}	Estimated at $z = 50$ m only. The sensitivities S_q and S_T of the CO_2 measurements to temperature and humidity are derived in Appendix C.
Temperature: Sensitivity of x_{CO_2} measurement: 50-m height turbulent flux Resulting bias	 $S_T = 0.42$ ppm K^{-1} $F_T = +0.25$ K m s^{-1} $F_{\mathrm{b},T} = +4{,}2$ µmol m^{-2} s^{-1}	
Total humidity and temperature bias	$F_{\mathrm{b}} < +3.1$ µmol m^{-2} s^{-1}	
Total bias	$F_b < +5$ µmol m^{-2} s^{-1}	

The temperature turbulent flux is expected to decrease with altitude and may even become negative (downward) near the top of the CBL (Behrendt et al., 2020). The humidity turbulent flux may increase slightly with altitude due to humidity entrainment at the CBL top (Behrendt et al., 2020; Giez et al., 1999). Since these fluxes introduce biases in the CO_2 flux measurements with opposite signs, the resulting bias is expected to decrease with altitude and may even become negative near the CBL top. We therefore consider that the bias values reported in Table 3 represent an upper bound for measurements in the lower and

https://doi.org/10.5194/egusphere-2026-4176
Preprint. Discussion started: 20 August 2026

middle portions of the CBL. We note that the biases introduced by temperature and humidity fluctuations constitute a significant source of error. Here, we bounded the bias for measurements in the lower portion of the CBL. Ideally, a precise determination of the vertical profile of CO_2 turbulent flux should be complemented by simultaneous measurements of the vertical profiles of humidity and temperature turbulent fluxes. Such measurements can be achieved using Raman lidar systems or DIAL lidar systems for humidity.

In conclusion of Sect. 4.3 and 4.4, the lidar achieves a random error of 11 µmol m^{-2} s^{-1} and a systematic error less than 5 µmol m^{-2} s^{-1} for a spatiotemporal resolution of 350 m and 4 hours. It corresponds to a global error, defined as the quadratic sum of the two errors, of 12 µmol m^{-2} s^{-1}.

5 Geophysical interpretation of measured CO_2 fluxes

The flux measurements are presented in Fig. 5. We apply vertical averaging to the flux measurements to reduce random error, so we present a vertical profile with two measurement points with a 350-m vertical integration. The random error is determined using the RS method presented in Sect. 4.3.3. We also report the 50-m height flux measurement performed by the SIRTA observatory.

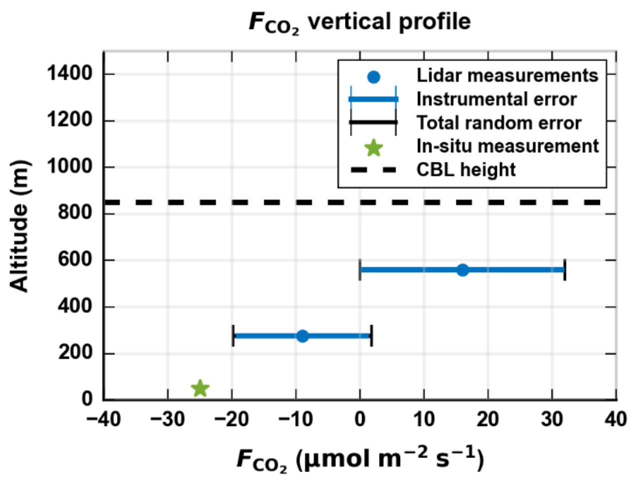

Figure 5 : CO_2 flux vertical profile with spatial averaging. The lowest point is averaged between 100 and 450 m and the highest point between 400 and 750 m. CBL: convective boundary layer.

The flux profile shows two measurements with opposite signs and a signal-to-noise ratio close to unity. Figure 6 presents the temporal evolution of these two measurements. Figures 6a and 6b show the temporal profiles of the measurements at the lowest elevations (100 – 450 m), and highest elevations (400 – 750 m) respectively, with a temporal resolution of 30 minutes. The random error is determined by the RS method. These temporal profiles support the temporal consistency of both measurements. At the lowest elevations (100 – 450 m), a negative flux of -9 ± 11 µmol m^{-2} s^{-1} is measured. This corresponds to a downward flux driven by the photosynthetic uptake from vegetation. The measured value is consistent with the flux measured by the

https://doi.org/10.5194/egusphere-2026-4176
Preprint. Discussion started: 20 August 2026

SIRTA observatory of − 25 µmol m^{-2} s^{-1} at 50 m, although the flux may decrease with altitude as the distance from the ground, which acts as the exchange interface, increases. At the highest elevations (400 – 750 m), a positive flux is detected, with a value of + 16 ± 16 µmol m^{-2} s^{-1}. This corresponds to an upward flux that cannot be explained by surface fluxes. This positive flux can be explained by a CO_2 concentration in the CBL that is higher than the concentration in the overlying residual layer (RL). This hypothesis is supported by the CO_2 concentration measurements from the ICOS station at Saclay, located 7 km away from the lidar site presented Fig. 7. The CO_2 concentration during our measurement period (426 ppm) is higher than the minimum CO_2 concentration observed at the end of the previous day before CBL formation (423 ppm around 19:00 local time). This minimum concentration is assumed to remain unchanged in the so-called residual layer, which is decoupled from the nocturnal boundary layer where CO_2 increases during the night.

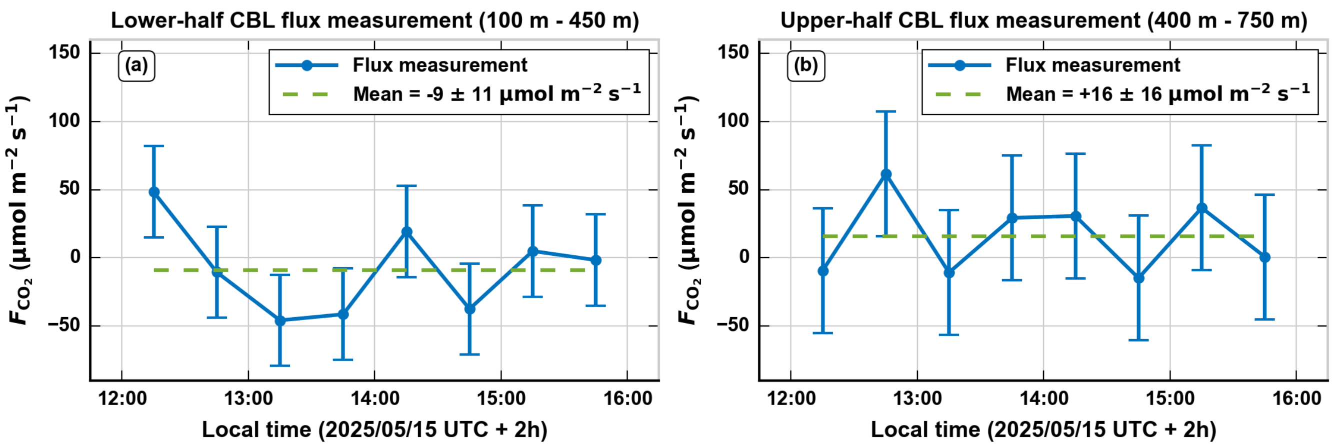

Figure 6 : Temporal series of flux measurement with a) 100 m to 450 m averaging b) 400 m to 750 m averaging.

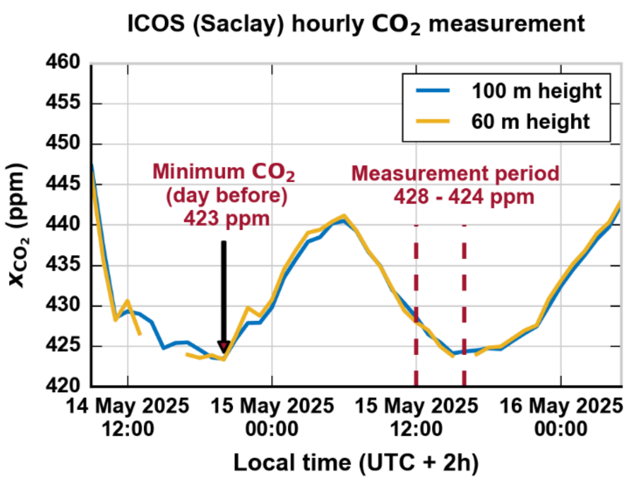

Figure 7 : Hourly CO_2 concentration measurement by the ICOS station at Saclay.

We also assume that the CBL was well mixed at the end of the previous day so that the concentration measured at the ICOS station corresponds to the average concentration in the CBL. The equality of the concentration measured at the two heights

https://doi.org/10.5194/egusphere-2026-4176
Preprint. Discussion started: 20 August 2026

(60 m and 100 m) supports this hypothesis. This analysis supports a decrease in CO_2 concentration with altitude across the CBL/RL interface, which would explain the positive flux measured at the top of the CBL.

6 Conclusion and Perspectives

We have presented the first set of measurements of CO_2 turbulent fluxes using a CDIAL lidar with random errors low enough to enable the study of fluxes driven by geophysical surface processes (such as photosynthesis) as well as by CBL entrainment. The random error in the flux estimates is primarily determined by the error in the CO_2 mixing-ratio measurements. The CDIAL lidar system benefits from its hybrid fiber/bulk amplification chain with single pass amplification, enabling a high pulse frequency and 1-mJ pulses. This architecture yields a random error of 30 ppm at spatiotemporal resolution of 13 s and 115 m, ranking among the lowest errors reported for CO_2 mixing ratio retrievals with a CDIAL lidar. This performance could be improved by replacing the pump laser of the Ho:YLF amplifier with a linearly polarized laser to optimize pump absorption. In addition, some sources of random error could be reduced by using higher-performance components, namely by lowering detector noise and the relative intensity noise of the local oscillator. These improvements could yield a 3-dB gain in CNR and would reduce random error in the CO_2 mixing ratio and flux estimates to 40 %.

We estimated the random error of flux measurements with an analytical expression derived through an analysis of the spatial correlation between flux estimates. This expression was validated using a statistical analysis of real flux measurements as well as Monte Carlo simulations based on the random shuffling (RS) method. Our results suggest that the RS method agrees more closely with the experimental results and may capture error contributions that are neglected by the analytical expression.

We applied this flux random error analysis to a measurement of a flux vertical profile within the CBL. We detect a downward flux in the lower part of the CBL and an upward flux in its upper part, which is consistent with measurements from the SIRTA observatory, and mixing-ratio measurements from the ICOS station. With a spatiotemporal resolution of 4 hour and 350 m the detection limit of the lidar was estimated at 11 µmol m^{-2} s^{-1} in the lower part of the CBL and of 16 µmol m^{-2} s^{-1} in its upper part.

In this study, we reached, for the first time with a CDIAL lidar, a detection limit that matches the geophysical signal. Future development should aim at lowering this detection limit to enable the retrieval of profiles with enhanced precision and resolution. This could be achieved through improvements to the hybrid laser system or by averaging repeated measurements over longer periods, such as a week or a month. Repeated observations would provide a better understanding of the CO_2 turbulent flux through the CBL, a key process governing the regional distribution of CO_2.

Appendix A : Flux random error expression

In this appendix, we derive the random error of the flux and its spatial correlation.

We first derive the expression for the flux random error. The fluctuations of CO_2 and wind x'_{CO_2} and w' are decomposed as follows:

https://doi.org/10.5194/egusphere-2026-4176
Preprint. Discussion started: 20 August 2026

$$x'_{\mathrm{CO_2}}(z_i,t) = x'_{\mathrm{CO_2,a}}(z_i,t) + x'_{\mathrm{CO_2,n}}(z_i,t) \tag{A1}$$

$$w' = w'_{\mathrm{a}}(z_i,t) + w'_{\mathrm{n}}(z_i,t) \tag{A2}$$

where $x'_{CO_2,\mathrm{a}}$ and w'_{a} denote the atmospheric turbulent fluctuations, $x'_{\mathrm{CO_2,n}}$ and w'_{n} denote the instrumental noise fluctuations. The result of the eddy-covariance calculation is (Behrend et al., 2020):

$$\rho_{\mathrm{d}}\frac{1}{N}\sum_{m=1}^{N} x'_{\mathrm{CO_2}}(z_i,m)w'(z_i,m) = F_{\mathrm{CO_2}} + \rho_{\mathrm{d}}\frac{1}{N}\left(\sum_{m=1}^{N} w'_{\mathrm{a}}(z_i,m).\,x'_{\mathrm{CO_2,n}}(z_i,m) + \sum_{m=1}^{N} w'_{\mathrm{n}}(z_i,m).\,x'_{\mathrm{CO_2,a}}(z_i,m) + \sum_{m=1}^{N} w'_{\mathrm{n}}(z_i,m).\,x'_{\mathrm{CO_2,n}}(z_i,m)\right) \tag{A3}$$

The three summation terms of the right-hand side represent the random error terms of the flux calculation. The standard deviation of this error is given by (Giez et al., 1999):

$$\sigma_{\mathrm{n},F}(z_i) = \rho_{\mathrm{d}}\sqrt{\frac{\Delta t}{T}}\sqrt{\sigma^2_{\mathrm{a},w}(z_i).\,\sigma^2_{\mathrm{n},x_{\mathrm{CO_2}}}(z_i) + \sigma^2_{\mathrm{n},w}(z_i).\,\sigma^2_{\mathrm{a},x_{\mathrm{CO_2}}}(z_i) + \sigma^2_{\mathrm{n},x_{\mathrm{CO_2}}}(z_i).\,\sigma^2_{\mathrm{n},w}(z_i)} \tag{A4}$$

Where $\sigma_{\mathrm{n},x_{\mathrm{CO_2}}}$ and $\sigma_{\mathrm{n},w}$ denote the instrumental random error standard deviations of $x_{\mathrm{CO_2}}$ and w respectively, while $\sigma_{\mathrm{a},x_{\mathrm{CO_2}}}$ and $\sigma_{\mathrm{a},w}$ correspond to their atmospheric turbulent standard deviations, Δt represents the temporal resolution of w and $x_{\mathrm{CO_2}}$ measurements, and T denotes the integration time used for the eddy-covariance flux measurement. The three terms under the square root correspond to the three error terms of A3. In our study, $\sigma^2_{\mathrm{n},x_{\mathrm{CO_2}}} \gg \sigma^2_{\mathrm{a},x_{\mathrm{CO_2}}}$ and $\sigma^2_{\mathrm{a},w}(z) \gg \sigma^2_{\mathrm{n},w}$. These considerations allow us to simplify Eq. (A4) and to obtain the random error expression used in this paper:

$$\sigma_{\mathrm{n},F}(z_i) = \rho_{\mathrm{d}}\sqrt{\frac{\Delta t}{T}}\,\sigma_{\mathrm{a},w}\sigma_{\mathrm{n},x_{\mathrm{CO_2}}}(z_i)\sigma_{\mathrm{n},x_{\mathrm{CO_2}}}(z_i) \tag{A5}$$

This implies that the dominant contribution to the flux error is the covariance between w'_{a} and $x'_{\mathrm{CO_2,n}}$. We therefore derive the spatial correlation of this leading error term. Let's introduce:

$$C_{z_i,z_j} = \rho^2_{\mathrm{d}}\mathrm{Cov}\left[\frac{1}{N}\sum_{m=1}^{N} w'_{\mathrm{a}}(z_i,m).\,x'_{\mathrm{CO_2,n}}(z_i,m)\,,\frac{1}{N}\sum_{m=1}^{N} w'_{\mathrm{a}}(z_j,m).\,x'_{\mathrm{CO_2,n}}(z_j,m)\right] \tag{A6}$$

Because the instrumental noise is temporally uncorrelated, the covariance of the product $w'_{\mathrm{a}}.\,x'_{\mathrm{CO_2,n}}$ is null when the temporal index m differs. This leads to:

$$C_{z_i,z_j} = \rho^2_{\mathrm{d}}\frac{1}{N^2}\sum_{m=1}^{N}\mathrm{Cov}\left[w'_{\mathrm{a}}(z_i,m).\,x'_{\mathrm{CO_2,n}}(z_i,m), w'_{\mathrm{a}}(z_j,m).\,x'_{\mathrm{CO_2,n}}(z_j,m)\right] \tag{A7}$$

We now introduce a simplifying assumption: we neglect the vertical variability of w'_{a} implying that the turbulent flux is driven by large eddy scales:

$$w'_{\mathrm{a}}(z_i,m) = w'_{\mathrm{a}}(z_j,m) \tag{A8}$$

Under this assumption, we can write:

$$C_{z_i,z_j} = \rho^2_{\mathrm{d}}\frac{1}{N^2}\sum_{m=1}^{N} w'_{\mathrm{a}}(z_j,m)^2\; Cov\left[x'_{\mathrm{CO_2,n}}(z_i,m), x'_{\mathrm{CO_2,n}}(z_j,m)\right] \tag{A9}$$

Let's introduce

$$C_{x_{\mathrm{CO_2}},z_i,z_j} = \mathrm{Cov}\left[x'_{\mathrm{CO_2,n}}(z_i,m), x'_{\mathrm{CO_2,n}}(z_j,m)\right] \tag{A10}$$

This covariance is supposed independent of the time index m. It leads to:

https://doi.org/10.5194/egusphere-2026-4176
Preprint. Discussion started: 20 August 2026

$$C_{z_i,z_j} = \rho_d^2 C_{x_{CO_2},z_i,z_j} \frac{1}{N^2} \sum_{m=1}^{N} w_a'\left(z_j, m\right)^2 \tag{A11}$$

Noting that $N = T/\Delta t$, and recognising the definition of $\sigma_{a,w}^2$, we obtain an expression analogous to that of the variance of flux random error:

$$C_{z_i,z_j} = \rho_d^2 \frac{\Delta t}{T} \sigma_{a,w}^2 C_{x_{CCO_2},z_i,z_j} \tag{A12}$$

The spatial correlation of the flux random error appears to be determined by that of x_{CO_2}. The spatial correlation of x_{CO_2} is derived separately in Appendix B. Using this results, the spatial correlation of the flux random error follows:

$$C_{z_i,z_j} = \begin{cases} -\rho_d^2 \frac{\Delta t}{T} \sigma_{a,w}^2 \frac{1}{(2WF)^2} \frac{1}{(2\Delta R)^2} \sigma(\tau(z_{i+1}))^2 & \text{if } z_j = z_{i\pm 2} \\ 0 & \text{else} \end{cases} \tag{A13}$$

Where $\sigma(\tau(z_i))$ denotes the random error standard deviation of the optical depth $\tau(z_i)$, and ΔR is the longitudinal resolution of the lidar. In parallel, we introduce an expression for the variance of the flux random error in the flux (see Appendix B):

$$\sigma_{n,F}^2(z_i) = \rho_d^2 \frac{\Delta t}{T} \sigma_{a,w}^2 \frac{1}{(2WF)^2} \frac{1}{(2\Delta R)^2} \left(\sigma(\tau(z_{i+1}))^2 + \sigma(\tau(z_{i-1}))^2\right) \tag{A14}$$

We now have all the elements required to derive the random error of a spatially averaged flux between the heights z_{min} and z_{max}.

$$\langle F_{CO_2} \rangle_{z_{min}}^{z_{max}} = \frac{1}{k} \sum_{z_i=z_{min}}^{z_{max}} F_{CO_2}(z_i) \tag{A15}$$

where k is the number of flux samples included in the vertical averaging. The variance of the averaged flux $\langle \sigma_{n,F}^2 \rangle_{z_{min}}^{z_{max}}$ is given by:

$$\langle \sigma_{n,F}^2 \rangle_{z_{min}}^{z_{max}} = \frac{1}{k^2} \left(\sum_{z_i=z_{min}}^{z_{max}} \sigma_{n,F}^2(z_i) + 2 \sum_{z_{min}<z_i<z_j<z_{max}} C_{z_i,z_j} \right) \tag{A16}$$

Using the structure of the covariance, we can write:

$$\langle \sigma_{n,F}^2 \rangle_{z_{min}}^{z_{max}} = \frac{1}{k^2} \left(\sum_{z_i=z_{min}}^{z_{max}} \sigma_{n,F}^2(z_i) + 2 \sum_{z_i=z_{min}}^{z_{max-2}} C_{z_i,z_{i+2}} \right) \tag{A17}$$

This yields:

$$\langle \sigma_{n,F}^2 \rangle_{z_{min}}^{z_{max}} = \frac{1}{k^2} \rho_d^2 \frac{\Delta t}{T} \sigma_{a,w}^2 \frac{1}{(2WF)^2} \frac{1}{(2\Delta R)^2} \left(\sum_{z_i=z_{min}}^{z_{max}} \left[\sigma\left(\tau(z_{i+1})\right)^2 + \sigma\left(\tau(z_{i-1})\right)^2\right] - 2 \sum_{z_i=z_{min}}^{z_{max-2}} \sigma(\tau(z_{i+1}))^2 \right) \tag{A18}$$

By expanding the telescoping sum, we obtain:

$$\langle \sigma_{n,F}^2 \rangle_{z_{min}}^{z_{max}} = \frac{1}{k^2} \rho_d^2 \frac{\Delta t}{T} \sigma_{a,w}^2 \frac{1}{(2WF)^2} \frac{1}{(2\Delta R)^2} \left(\sigma(z_{max+1})^2 + \sigma(z_{max-1})^2 + \sigma(z_{min+1})^2 + \sigma(z_{min-1})^2 \right) \tag{A19}$$

By recognizing the expression of $\sigma_{n,x_{CO_2}}^2$, we obtain:

$$\langle \sigma_{n,F}^2 \rangle_{z_{min}}^{z_{max}} = \frac{1}{k^2} \rho_d^2 \frac{\Delta t}{T} \sigma_{a,w}^2 \left(\sigma_{n,x_{CO_2}}^2(z_{max}) + \sigma_{n,x_{CO_2}}^2(z_{min}) \right) \tag{A20}$$

Under the hypothesis that w_a' is spatially invariant, Eq. (A5) yields the random error in fluxes after spatial averaging:

$$\langle \sigma_{n,F}^2 \rangle_{z_{min}}^{z_{max}} = \frac{1}{k} \sqrt{\sigma_{n,F}(z_{max})^2 + \sigma_{n,F}(z_{min})^2} \tag{A21}$$

https://doi.org/10.5194/egusphere-2026-4176
Preprint. Discussion started: 20 August 2026

Appendix B: spatial correlation of the random error on CO_2 mixing ratio

We derive the spatial correlation of the random error affecting $x_{\mathrm{CO_2}}$. A measurement of $x_{\mathrm{CO_2}}(z_i)$; is derived by a linear regression on $\tau(z_{i-1}), \tau(z_i)$ and $\tau(z_{i+1})$, over a distance of $2\Delta R$. We use a simplified expression for $x_{\mathrm{CO_2}}$, in which the differential absorption is computed after the two measurements of τ located at the edges of the range gate :

$$x_{\mathrm{CO_2}}(z_i) = \frac{1}{2WF}\frac{\tau(z_{i+1}) - \tau(z_{i-1})}{2\Delta R} \quad \text{(B1)}$$

where $\tau(R_i)$ denotes the optical depth at range gate R_i and δr denotes the spatial resolution of τ. The first neighbouring estimate of $x_{\mathrm{CO_2}}(z_i)$ is given by:

$$x_{\mathrm{CO_2}}(z_{i+1}) = \frac{1}{2WF}\frac{\tau(z_{i+2}) - \tau(z_i)}{2\Delta R} \quad \text{(B2)}$$

It appears that $x_{\mathrm{CO_2}}(z_{i+1})$ is computed from optical depth measurements that are different of those used for $x_{\mathrm{CO_2}}(z_i)$. The independence of the optical depth random errors therefore implies:

$$C_{x_{\mathrm{CO_2}}, z_i, z_{i+1}} = 0 \quad \text{(B3)}$$

The second neighbouring estimate of $x_{\mathrm{CO_2}}(z_i)$ is:

$$x_{\mathrm{CO_2}}(z_{i+2}) = \frac{1}{2WF}\frac{\tau(z_{i+3}) - \tau(z_{i+1})}{2\Delta R} \quad \text{(B4)}$$

The covariance between the $x_{\mathrm{CO_2}}$ estimates is:

$$C_{x_{\mathrm{CO_2}}, z_i, z_{i+2}} = \frac{1}{(2WF)^2}\frac{1}{(2\Delta R)^2}\mathrm{Cov}[\tau(z_{i+3}) - \tau(z_{i+1}), \tau(z_{i+1}) - \tau(z_{i-1})] \quad \text{(B5)}$$

Expanding this expression yields:

$$C_{x_{\mathrm{CO_2}}, z_i, z_{i+2}} = \frac{1}{(2WF)^2}\frac{1}{(2\Delta R)^2}(-1).\mathrm{Cov}[\tau(z_{i+1}), \tau(z_{i+1})] \quad \text{(B6)}$$

We obtain:

$$C_{x_{\mathrm{CO_2}}, z_i, z_{i+2}} = -\frac{1}{(2WF)^2}\frac{1}{(2\Delta R)^2}\sigma(\tau(z_{i+1}))^2 \quad \text{(B7)}$$

where $\sigma(\tau(z_i))$ is the standard deviation of random error in $\tau(z_i)$. For all other x_{CO_2} estimates, the optical depth do not overlap with those of $x_{CO_2}(z_i)$ and the covariance is therefore null. In conclusion:

$$C_{x_{\mathrm{CO_2}} z_i, z_j} = \begin{cases} -\frac{1}{(2WF)^2}\frac{1}{(2\Delta R)^2}\sigma(\tau(z_{i+1}))^2 & \text{if } z_j = z_{i\pm 2} \\ 0 & \text{else} \end{cases} \quad \text{(B8)}$$

In parallel, we introduce a useful expression for the variance of the flux random error in the flux according to Eq. (B1):

$$\sigma_{\mathrm{n}, x_{\mathrm{CO_2}}}(z_i) = \frac{1}{(2WF)^2}\frac{1}{(2\Delta R)^2}((\tau(z_{i+1}))^2 + \sigma(\tau(z_{i-1}))^2 \quad \text{(B9)}$$

Appendix C : Evaluation of the sensitivities of x_{CO_2} and F_{CO_2} to the atmospheric parameters.

The $x_{\mathrm{CO_2}}$ measurements are computed using atmospheric parameters denoted by X, representing either T or q. If the true atmospheric deviates by a small amount X', the resulting bias in the $x_{\mathrm{CO_2}}$ retrieval $x_{\mathrm{CO_2,b},X}$ is:

https://doi.org/10.5194/egusphere-2026-4176
Preprint. Discussion started: 20 August 2026

$$x_{\mathrm{CO_2,b},X} = x_{\mathrm{CO_2}}(X) - x_{\mathrm{CO_2}}(X + X') \quad \text{(C1)}$$

Equivalently,

$$x_{\mathrm{CO_2,b},X} = -\frac{\partial x_{\mathrm{CO_2}}}{\partial X} X' \quad \text{(C2)}$$

Let $S_X = -\frac{\partial x_{\mathrm{CO_2}}}{\partial X}$ denote the sensitivity of the $x_{\mathrm{CO_2}}$ measurement to a fluctuation of the atmospheric parameter. Then:

$$x_{\mathrm{CO_2,b},X} = S_X X' \quad \text{(C3)}$$

When the bias term is included in the eddy-covariance flux calculation (Eq. (5)), an additional contribution appears, corresponding to the bias in the flux estimate.

$$F_{\mathrm{CO_2,b},X}(z) = \rho_{\mathrm{d}} S_X \frac{1}{N} \sum_{m=1}^{N} w'(z,m) X'(z,m) \quad \text{(C4)}$$

We now derive the expression of the sensitivities S_X . Let us consider the expression of $x_{\mathrm{CO_2}}$ (Eq. (2)), where $WF = N_A . \rho_{\mathrm{d}}(T,q,p) . (\tilde{\sigma}_{\mathrm{ON}}(T,p) - \tilde{\sigma}_{\mathrm{OFF}}(T,p))$ denotes the so-called Weighting Function, and α (m^{-1}) the differential absorption :

$$x_{\mathrm{CO_2}}(z_i) = \frac{1}{WF(T,q,p)} . \alpha(z_i) \quad \text{(C5)}$$

Differentiating with respect to X yields:

$$\frac{\partial x_{\mathrm{CO_2}}}{\partial X} = -\frac{1}{WF^2} . \frac{\partial WF}{\partial X} . \alpha(z_i) \quad \text{(C6)}$$

Recognizing the expression of $x_{\mathrm{CO_2}}$, we obtain:

$$S_X = \frac{1}{WF} . \frac{\partial WF}{\partial X} \langle x_{\mathrm{CO_2}} \rangle \quad \text{(C7)}$$

assuming a mean atmospheric mixing ration of $\langle x_{\mathrm{CO_2}} \rangle = 426$ ppm. The sensitivity of $x_{\mathrm{CO_2}}$ to temperature S_T (ppm K^{-1}) is computed using the algorithm presented in Sect. 2.1. We evaluate the derivative of WF by computing its change for a 1-K perturbation from a mean temperature of 10°C, which yields $S_T = 0.42$ ppm K^{-1}. The sensitivity of $x_{\mathrm{CO_2}}$ to specific humidity S_q (ppm g^{-1} kg) is derived analytically by differentiating ρ_{d} (Eq. (4)) with respect to q:

$$S_q = -\frac{\frac{M_{\mathrm{d}}}{M_{\mathrm{H_2O}}}}{1 + q\frac{M_{\mathrm{d}}}{M_{\mathrm{H_2O}}}} \langle x_{\mathrm{CO_2}} \rangle \quad \text{(C8)}$$

which gives $S_q = -0.66$ ppm g^{-1} kg.

Data Availability

The lidar and in situ data are available on request from the authors

https://doi.org/10.5194/egusphere-2026-4176
Preprint. Discussion started: 20 August 2026

Author contribution

Mathys Thiers carried out the experimental setup, the atmospheric measurements, and the data analysis. Nicolas Cézard, Julien Lahyani, and Fabien Gibert developed the hybrid laser emitter and contributed to the setup and validation of the CDIAL lidar. Fabien Gibert provided expertise in the geophysical interpretation of flux measurements. Mathys Thiers prepared the manuscript with contributions from all co-authors.

Competing interest

The authors declare they have no conflict of interest.

Acknowledgement

The authors would like to thank SIRTA and the ICOS station of Saclay for providing the in situ and remote sensing data used in this study.

Financial support

This study was funded by the Office National d'Études et de Recherches Aérospatiales (projects Atmosphère and ROSALI).

References

Behrendt, A., Wulfmeyer, V., Senff, C., Muppa, S. K., Späth, F., Lange, D., Kalthoff, N., and Wieser, A.: Observation of sensible and latent heat flux profiles with lidar, Atmos. Meas. Tech., 13**,** 3221–3233, doi:10.5194/amt-13-3221-2020, 2020.

Berger, B. W., Davis, K. J. and Yi, C.: Long-term carbon dioxide fluxes from a very tall tower in a northern forest: flux measurement methodology, J. Atmos. Ocean. Tech., 18, 529-542, 2001.

Billesbach, D. P.: Estimating uncertainties in individual eddy covariance flux measurements: A comparison of methods and a proposed new method, Agricultural and Forest Meteorology, Volume 151, Issue 3, 394-405, https://doi.org/10.1016/j.agrformet.2010.12.001, 2011.

Burba, G.: Eddy covariance method for scientific, industrial, agricultural and regulatory applications: a field book on measuring ecosystem gas exchange and areal emission rates, LI-COR Biosciences, ISBN 978-0-615-76827-4, 2013.

Delwiche, K. B., Nelson, J., Kowalska, N., Moore, C. E., Shirkey, G., Tarin, T., Cleverly, J. R., and Keenan, T. F.: Charting the future of the FLUXNET network, Bull. Amer. Meteor. Soc., 105, E466–E473, doi:10.1175/BAMS-D-23-0316.1, 2024.

Di Girolamo, P., Marchese, R., Whiteman, D. N., and Demoz, B. B.: Rotational Raman lidar measurements of atmospheric temperature in the UV, Geophys. Res. Lett., 31, L01106, https://doi.org/10.1029/2003GL018342, 2004.

https://doi.org/10.5194/egusphere-2026-4176
Preprint. Discussion started: 20 August 2026

Engelmann, R., Wandinger, U., Ansmann, A., Müller, D., Žeromskis, E., Althausen, D., and Wehner, B.: Lidar observations of the vertical aerosol flux in the planetary boundary layer, J. Atmos. Oceanic Technol., 25, 1296–1306, doi:10.1175/2007JTECHA967.1, 2008.

Gibert, F., Flamant, P. H., Bruneau, D., and Loth, C.: Two-micrometer heterodyne differential absorption lidar measurements of the atmospheric CO_2 mixing ratio in the boundary layer, Appl. Opt., 45, 4448–4458, doi:10.1364/AO.45.004448, 2006.

Gibert, F., Flamant, P. H., Cuesta J., and Bruneau, D.: Vertical 2-µm heterodyne differential absorption lidar measurements of mean CO_2 mixing ratio in the troposphere. J. Atmos. Oceanic Technol., 25, 1477–1497, https://doi.org/10.1175/2008JTECHA1070.1, 2008.

Gibert, F., Koch, G. J., Beyon, J. Y., Hilton, T. W., Davis, K. J., Andrews, A., Flamant, P. H., and Singh, U. N.: Can CO_2 turbulent flux be measured by lidar? A preliminary study, J. Atmos. Oceanic Technol., 28, 365–377, doi:10.1175/2010JTECHA1446.1, 2011.

Gibert, F., Edouart, D., Monnier, P., Collignan, J., Lopez, J., and Cénac, C.: Scalar turbulent fluxes and variances in the interfacial layer from lidar observations and assessment of Lagrangian stochastic models, Q. J. R. Meteorol. Soc., 152, e70016, https://doi.org/10.1002/qj.70016, 2026.

Giez, A., Ehret, G., Schwisow, R. L., Davis, K. J. and Lenschow, D. H.: Water vapor flux measurements from ground-based vertically pointed water vapor Differential Absorption and Doppler Lidars, J. Atmos. Ocean. Tech., 16, 237-250, https://doi.org/10.1175/1520-0426(1999)016%3C0237:WVFMFG%3E2.0.CO;2, 1999.

Haeffelin, M., Barthès, L., Bock, O., Boitel, C., Bony, S., Bouniol, D., Chepfer, H., Chiriaco, M., Cuesta, J., Delanoë, J., Drobinski, P., Dufresne, J.-L., Flamant, C., Grall, M., Hodzic, A., Hourdin, F., Lapouge, F., Lemaître, Y., Mathieu, A., Morille, Y., Naud, C., Noël, V., O'Hirok, W., Pelon, J., Pietras, C., Protat, A., Romand, B., Scialom, G., and Vautard, R.: SIRTA, a ground-based atmospheric observatory for cloud and aerosol research, Ann. Geophys., 23, 253–275, https://doi.org/10.5194/angeo-23-253-2005, 2005.

Hannun, R. A., Wolfe, G. M., Kawa, S. R., Hanisco, T. F., Newman, P. A., Alfieri, J. G., Barrick, J., Clark, K. L., DiGangi, J. P., Diskin, G. S., King, J., Kustas, W. P., Mitra, B., Noormets, A., Nowak, J. B., Thornhill, K. L., and Vargas, R.: Spatial heterogeneity in CO_2, CH_4, and energy fluxes: insights from airborne eddy covariance measurements over the Mid-Atlantic region, Environ. Res. Lett., 15, 035008, doi:10.1088/1748-9326/ab7391, 2020.

Lahyani, J., Thiers, M., Gibert, F., Edouart, D., Le Gouët, J., and Cézard, N.: Hybrid fiber/bulk laser source designed for CO_2 and wind measurements at 2.05 µm, Opt. Lett., 49, 969–972, doi:10.1364/OL.49.000969, 2024.

Lenschow, D. H., Mann, J., and Kristensen, L.: How long is long enough when measuring fluxes and other turbulence statistics?, J. Atmos. Oceanic Technol., 11, 661–673, doi:10.1175/1520-0426(1994)011<0661:HLILEW>2.0.CO;2, 1994.

Lenschow, D. H., Wulfmeyer, V., and Senff, C.: Measuring second- through fourth-order moments in noisy data, J. Atmos. Oceanic Technol., 17, 1330–1347, doi:10.1175/1520-0426(2000)017<1330:MSTFOM>2.0.CO;2, 2000.

Miyazaki, K., Patra, P. K., Takigawa, M., Iwasaki, T., and Nakazawa, T.: Global-scale transport of carbon dioxide in the troposphere, J. Geophys. Res., 113, D15301, doi:10.1029/2007JD009557, 2008.

https://doi.org/10.5194/egusphere-2026-4176
Preprint. Discussion started: 20 August 2026

Ramonet, M., Charrondière, C., Delmotte, M., Lopez, M.: ICOS ATC NRT CO2 growing time series from Saclay (60.0 m), 2025-04-01–2026-06-12, ICOS RI, https://hdl.handle.net/11676/yYiaSgVwTfx_HvOdXc8TUDrF, 2026.

Rannik, Ü., Peltola, O., and Mammarella, I.: Random uncertainties of flux measurements by the eddy covariance technique, Atmos. Meas. Tech., 9, 5163–5181, https://doi.org/10.5194/amt-9-5163-2016, 2016.

Rye, B. J.: Estimate optimization parameters for incoherent backscatter heterodyne lidar including unknown return signal bandwidth, Appl. Opt., 39, 6086–6096, doi:10.1364/AO.39.006086, 2000.

Senff, C., Bösenberg, J. and Peters G.: Measurement of water vapor flux profiles in the convective boundary layer with lidar and radar-RASS, J. Atmos. Ocean. Tech., 11, https://doi.org/10.1175/1520-0426(1994)011%3C0085:MOWVFP%3E2.0.CO;2, 1994.

Stull, R. B.: Convective mixed layer, in: An Introduction to Boundary Layer Meteorology, edited by Stull, R. B., Springer Netherlands, Dordrecht, 441–497, https://doi.org/10.1007/978-94-009-3027-8_11, 1988.

Webb, E. K., Pearman, G. I., and Leuning, R.: Correction of flux measurements for density effects due to heat and water vapour transfer, Q. J. R. Meteorol. Soc., 106, 85–100, https://doi.org/10.1002/qj.49710644707, 1980.

Wulfmeyer, V., Muppa, S. K., Behrendt, A., Hammann, E., Späth, F., Sorbjan, Z., Turner, D. D., and Hardesty, R. M.: Determination of convective boundary layer entrainment fluxes, dissipation rates, and the molecular destruction of variances: theoretical description and a strategy for its confirmation with a novel lidar system synergy, J. Atmos. Sci., 73, 667–692, doi:10.1175/JAS-D-14-0392.1, 2016.